RESEARCH ARTICLE

Temperature- and stress-dependent electromechanical properties of phase-boundary-engineered KNN-based piezoceramics

Ahmed Gadelmawla[1] | Udo Eckstein[1] | Kevin Riess[1] | Yi-Xuan Liu[2] |
Ke Wang[2] | Jing-Feng Li[2] | Ken-ichi Kakimoto[3] | Neamul H. Khansur[1] |
Kyle G. Webber[1]

[1]Department of Materials Science and Engineering, Friedrich-Alexander-Universität Erlangen-Nürnberg, Erlangen, Germany

[2]State Key Laboratory of New Ceramics and Fine Processing, School of Materials Science and Engineering, Tsinghua University, Beijing, P. R. China

[3]Department of Life Science and Applied Chemistry, Graduate School of Engineering, Nagoya Institute of Technology, Nagoya, Japan

Correspondence
Ahmed Gadelmawla, Department of Materials Science and Engineering, Friedrich-Alexander-Universität Erlangen-Nürnberg, Erlangen, Germany.
Email: ahmed.gadelmawla@fau.de

Abstract
The influence of stress on the small-signal dielectric permittivity and piezoelectric coefficient of polycrystalline lead-free perovskite $0.92(Na_{1/2}K_{1/2})NbO_3 - (0.08 - x)Bi_{1/2}Li_{1/2}TiO_3 - xBaZrO_3$ (x = 0, 0.02, 0.04, 0.06, and 0.07) was characterized under different constant uniaxial stress up to -200 MPa within a temperature range of -150 to $450°C$, revealing stress-induced suppression of the electromechanical response as well as shifts in the phase boundaries. For all compositions, the interferroelectric and ferroelectric–paraelectric phase transitions were shifted to higher temperatures under the uniaxial compressive stress. Interestingly, the sensitivity to the applied stress was found to increase with increasing BZ/BLT ratio in the system. The origin of a different extent of stress-sensitivity with BZ/BLT ratio is suggested to be related to the change in the crystal structure. Additionally, at temperatures below $-50°C$, the relative permittivity showed a significant increase under applied compressive stress.

KEYWORDS
electromechanical properties, ferroelectricity, KNN–BLT–BZ, lead-free ferroelectrics

1 | INTRODUCTION

$(K_xNa_{1-x})NbO_3$ (KNN) has been investigated for several decades as a possible replacement for lead-containing compositions [1,2] due to the reported high Curie temperature, T_C, and relatively large piezoelectric coefficient (>100 pC/N), high acoustic vibration velocities, and low density. [3,4] In particular, piezoelectric coefficients (d_{33} = 416 pC/N) comparable to Pb(Zr,Ti)O_3 for textured Li, Ta, and Sb-doped KNN have been observed. [5] KNN is

a solid solution of the two end members of orthorhombic symmetry $KNbO_3$ (*Amm*2) and $NaNbO_3$ (*Pbcm*). At room temperature, the optimum electromechanical properties have been observed in the vicinity of the phase boundary separating the orthorhombic phases, namely, $K_{0.5}Na_{0.5}NbO_3$,[6] where the average crystallographic structure of $K_{0.5}Na_{0.5}NbO_3$ is considered orthorhombic (*Amm*2). However, there remains debate in the literature about the nature of the phase.[3,7–14] In addition to Wang and Li, who demonstrated that the perovskite-type ABO_3 subcell of KNN possesses monoclinic symmetry,[15] researchers have suggested that the room-temperature structure is monoclinic *Pm*.[14,16] Nevertheless, with decreasing temperature from the nonpolar cubic $Pm\bar{3}m$ symmetry, there is a phase transition to tetragonal (T) *P4mm* at 420°C, orthorhombic (O) *Amm*2 at 220°C, and rhombohedral (R) *R3c* at approximately −123°C. It is known that the orthorhombic–tetragonal phase boundary, which occurs in the vicinity of room temperature, is critical to these properties.[17] Here, a broad multiphase region has been demonstrated to be the origin of the nearly temperature-insensitive ferroelectric properties over a wide temperature range.[4,18]

It has been demonstrated, however, that the phase-boundary region can be engineered through chemical substitution on the A- and B-site leading to a wider multiphase region[3] and the formation of an R–T phase boundary,[17,19] both of which have been suggested to enhance the electromechanical properties.[4] Although many chemical substitutions shift the T_{R-O}, T_{O-T}, and T–C phase boundaries to lower temperatures, as shown by Li et al.,[4] certain chemical elements have been found to increase phase transition temperatures, allowing for the tuning of the phase regions T_{R-O} and T_C.[3] For example, Li shifts the ferroelectric–paraelectric phase transition T_C to a higher temperature,[20] whereas zirconates, such as $BaZrO_3$, increase the T_{R-O} phase boundary as larger B cations favor the lower temperature phase. As such, simultaneous chemical modification of the T_{R-O} and T_{O-T} phase boundaries is a promising approach to improving the functional properties of KNN-based materials by establishing the R–T phase boundary at room temperature.[17,21] This strategy has already reported compositions with enhanced functional properties and temperature stability.[22] It should be noted that the exceptional functional properties of PZT are often attributed to the existence of mixed R and T phases at room temperature and the vertical nature of the R–T phase boundary.[23]

Among the reported KNN-based compositions with chemically engineered R–T phase boundaries at room temperature,[21] compositions containing $Bi_{1/2}Li_{1/2}TiO_3$ and $BaZrO_3$ show excellent piezoelectric properties.[24] Importantly, the phase boundary and associated functional properties can easily be tuned by changing the $Bi_{1/2}Li_{1/2}TiO_3$ and $BaZrO_3$ ratio, that is, $0.92(Na_{0.5}K_{0.5})NbO_3–(0.08 − x)Bi_{1/2}Li_{1/2}TiO_3–xBaZrO_3$ (KNN–100*x*BZ, where *x* = 0, 0.02, 0.04, 0.06, and 0.07). For example, previous works have shown a maximum room temperature piezoelectric coefficient, d_{33} = 348 pC/N for *x* = 0.06, where compositionally tuned the coexistence of rhombohedral and tetragonal phases is present at room temperature.[24] However, the influence of varying external fields, such as a change in temperature and mechanical stress on the piezoelectric coefficients, are not well understood. It should be noted that substitution of A and B-cations in ABO_3-perovskites with different ionic radii can induce a change in the internal chemical pressure, akin to externally applied hydrostatic pressure.

It is well known that external mechanical fields can shift phase-transition boundaries in perovskite ferroelectrics, which can be used to tune functional properties,[25] induce new phases in thin films,[26] or create a morphotropic phase boundary.[27] In addition, through tailoring of the microstructure, the internal stress can also enhance the dielectric response.[28] The previous work has shown that uniaxial[29] and biaxial[30] compressive stresses increase the Curie point through the stabilization of the lower symmetry polar phase, whereas hydrostatic stress leads to a stabilization of the higher temperature cubic phase that reduces T_c.[31,32] These mechanical fields can act analogously to a chemical substitution, which are known to exert a chemical pressure that can shift phase boundaries depending on the relative size of the dopant cations.[32,33]

The importance of chemically tuning the phase boundaries has also been identified in KNN-based materials.[4] This led to the suggestion in subsequent investigations in the KNN-based materials that chemically tuning the rhombohedral–orthorhombic phase boundary to higher temperatures and the orthorhombic–tetragonal phase to lower temperatures would eventually result in the exclusion of the orthorhombic phase all together and a rhombohedral–tetragonal phase boundary near room temperature.[17,24,34] This is particularly interesting, as the R–T phase boundary has been suggested to be responsible for the enhanced electromechanical properties observed in numerous ferroelectric material systems, most notably $Pb(Zr,Ti)O_3$.[23] There are, however, limited studies on the influence of stress on the stable phase in KNN-based compositions, although the previous work has shown that mechanical fields can induce a shift of the interferroelectric O–T phase transition as well as the ferroelectric–paraelectric Curie point.[35,36] For example, a stress-dependent Raman study of Li-doped KNN reported a shift in the O–T phase transition to room temperature under hydrostatic pressure, the increase of Li content in the system leads to lower symmetry and therefore shifts the phase transition to a higher pressure value.[37] In

contrast, applied uniaxial compressive stress has been shown to stabilize lower symmetry phases,[35,38–41] resulting in an increase in both interferroelectric and ferroelectric–paraelectric phase boundaries.

Nevertheless, despite the numerous developments in optimizing the electromechanical properties of KNN-based materials, very few reports are available on the influence of mechanical stress on the functional properties either at room temperature or at a higher temperature.[35,42–44] Such investigations are important for practical applications of functional materials as they experience a harsh environment, that is, under high stress and temperature. As such, in this work, stress- and temperature-dependent functional properties of a series of $0.92(Na_{0.5}K_{0.5})NbO_3$–$(0.08 - x)Bi_{1/2}Li_{1/2}TiO_3$–$xBaZrO_3$ ($x = 0$, 0.02, 0.04, 0.06, and 0.07, KNN–xBZ) were investigated to reveal the influence of mechanical stress on the temperature-dependent functional properties as well as the O–T and R–T phase boundaries. Importantly, this work comprehensively demonstrates the influence of uniaxial mechanical stress on the chemically tuned phase boundaries and functional piezoelectric response of KNN-based compositions.

2 | EXPERIMENTAL METHODOLOGY

Lead-free polycrystalline $0.92(Na_{0.5}K_{0.5})NbO_3$–$(0.08 - x)Bi_{1/2}Li_{1/2}TiO_3$–$xBaZrO_3$ + 1 wt.% MnO_2 ($x = 0$, 0.02, 0.04, 0.06, and 0.07) was fabricated by the conventional solid-state processing route. The raw materials K_2CO_3 (99.9%), Na_2CO_3 (99.9%), Nb_2O_5 (99.99%), Bi_2O_3 (99.9%), Li_2CO_3 (99%), TiO_2 (99.99%), $BaCO_3$ (99.99%), and ZrO_2 (99.9%) were mixed in stoichiometric proportions and milled in a planetary mill (P-7, Fritsch, Idar-Oberstein, Germany). All compositions were doped with 1 wt.% MnO_2. Following this, the resulting powders were calcined at 1000°C for 5 h and subsequently sintered between 1140 and 1160°C, depending on the compositions, for 5 h. Additional details of the synthesis can be found elsewhere.[12,24]

For microstructure analysis, samples were first ground using an 18 μm grinding disc to ensure flatness. Subsequent polishing steps of 9, 6, 3, and 1 μm were performed using respective polishing pads and diamond suspension, with a final polishing step with silica oxide polishing suspension. The microstructure images were collected using a scanning electron microscope (Helios NanoLab 600i FIB Workstation, FEI Company, Oregon, USA) at a magnifications of 1250–5000×. Grain size analysis was performed using ImageJ software,[45] on minimum 3 micrographs of respective samples, where at least 100 grains were measured per micrograph.

Following sintering, cylindrical samples were ground to 0.500 mm (±0.01 mm) in height and 5.8 mm (±0.01 mm) in diameter with a surface grinder. Following this, Pt electrodes of approximately 70 nm thickness were sputtered on the two opposing 5.8 mm circular faces for stress- and temperature-dependent dielectric and piezoelectric measurements. The sputtered samples were kept at 120°C for 2 h before applying an electric field to avoid issues related to moisture content. The samples were poled in a silicone oil bath at 120°C for 30 min with an applied electric field of 4 kV/mm and subsequent field cooling to ∼25°C.

A screw-type load frame (Instron 5967, Instron GmbH, Germany) with an integrated cooling and heating chamber was used for the electromechanical experiments. The experimental setup was presented in previous works.[46,47] For electrical contacts, two tungsten carbide loading dies were attached to the samples for uniaxial stress. The load frame software (Bluehill LE Software, Instron) was used to control the load and loading rate by supporting constant compressive stress between −5 and −200 MPa, whereas the samples were heated from −150 to 450°C at a rate of 2 K/min. Liquid N_2 was used to cool the samples down to −150°C in a thermal chamber (TK 26.600.LN2, Fresenberger). This equipment is based on an integrated piezoelectric actuator (P-025.80, PI Ceramic GmbH, Germany) that partially loaded the sample using a sinusoidal waveform with an amplitude of ±0.5 MPa at various frequencies between 0.5 and 140 Hz. A custom Lab-VIEW program was developed to control and evaluate the obtained data.[47]

3 | RESULTS AND DISCUSSION

Microstructure analysis revealed that the average grain size for samples with low BZ content showed unhomogenized grain size distribution compared to those with higher BZ content (see Figure S1). For example, in the case of KNN–0BZ and KNN–2BZ, the grain-size distributions were bimodal showing smaller average grain sizes of 1.3 ± 2.19 and 1.64 ± 1.41 μm, respectively, as well as a larger average grain size of 10.54 ± 3.77 and 7.06 ± 2.11 μm, respectively. A similar grain size distribution effect has been observed for Li- and Ta-modified KNN ceramics.[48–51] In contrast, the average grain size for high BZ content samples showed single grain size distribution, where KNN–4BZ and KNN–7BZ displayed average grain size ranges of 2.72 ± 1.35 and 1.80 ± 0.72 μm, respectively. Interestingly, however, KNN–6BZ grain size showed a sudden unhomogenized increase of some grains as a phenocryst effect, which was determined by a bimodal distribution with 1.47 ± 1.01 μm for the matrix and 5.90 ± 2.10 μm for the large grains, although the origins for this behavior remain
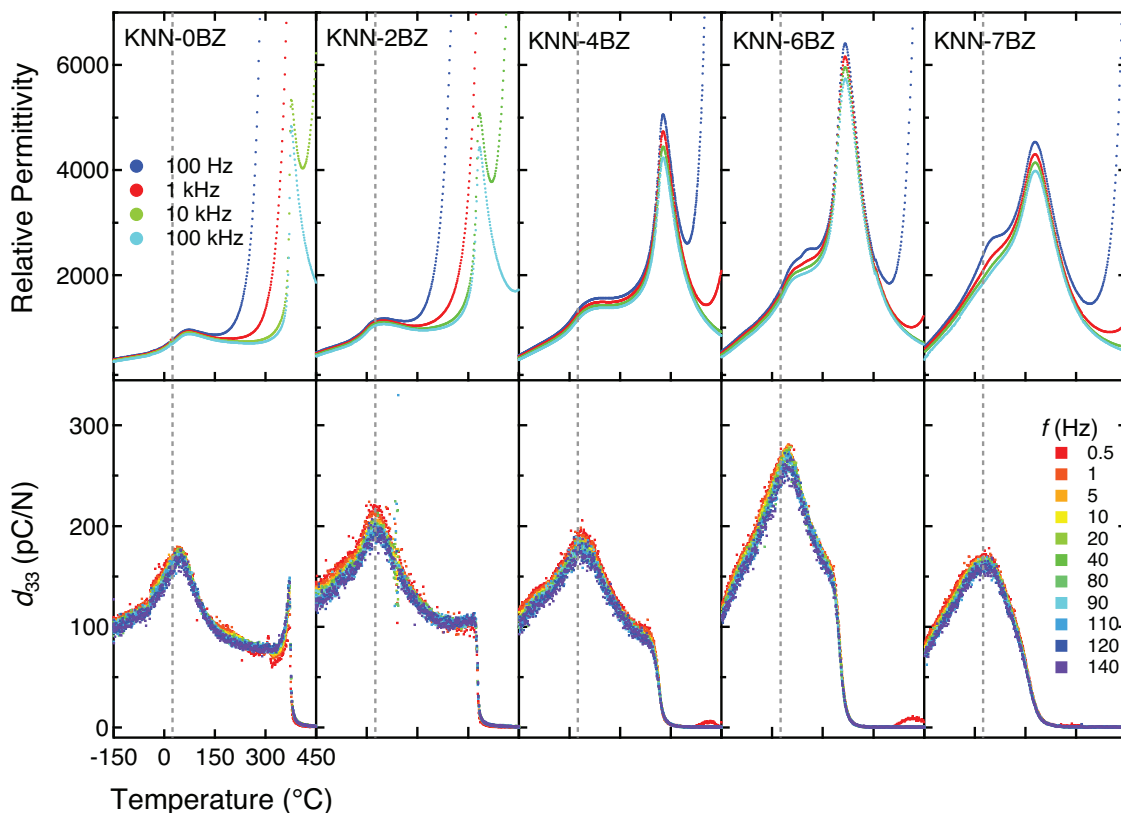
FIGURE 1 The relative permittivity (top row) and piezoelectric coefficient d_{33} (bottom row) of KNN–xBZ under −5 MPa (i.e., x = 0, 2, 4, 6, and 7). Gray dashed lines indicate 25°C.

unclear. Interestingly, pores were observed primarily along the grain boundaries, which increased with increasing BZ content. In addition, the relative density range for all samples was 98.3%–98.7%.

The temperature-dependent small-signal dielectric and piezoelectric properties were investigated for KNN–$100x$BZ (x = 0, 0.02, 0.04, 0.06, and 0.07) from −150 to 450°C under −5 MPa uniaxial stress as a function of frequency (Figure 1). A bias stress was applied during measurements to ensure the electrical and mechanical contact of the sample during measurement. Previous reports, however, show that a uniaxial stress of −5 MPa as equivalent to the stress-free state for PZT and Li-doped KNN,[40,47] as the macroscopic critical stress field required to induce domain switching or other nonlinear, hysteretic processes in these ceramic compositions is at least an order of magnitude higher than the applied bias stress. Following the electrical poling procedure, the piezoelectric coefficient d_{33} was measured at room temperature with a Berlincourt meter (PiezoMeter System PM300) using a mechanical force of 11 N and frequency of 110 Hz for KNN–0BZ, 2BZ, 4BZ, 6BZ, and 7BZ, revealing values of 150, 173, 160, 242, and 145 pC/N, respectively. These d_{33} values correspond well to the observed measured d_{33} values under −5 MPa, which were 157, 190, 169, 246, and 160 pC/N, confirming

that the −5 MPa prestress did not significantly alter the poled state at room temperature. Please note, the d_{33} value of the respective compositions reported in the previous work is slightly different than that of our measured value. The difference in d_{33} could be related to the difference in processing condition as well as the poling conditions. Nevertheless, the focus of this work, that is, stress-induced variation in polymorphic phase boundaries should not be affected by the variation in d_{33} value.

The temperature-dependent dielectric and piezoelectric responses (Figure 1) show several interesting phenomena with variations in the BZ/BLT ratio. First, at low BZ content, there is a frequency dependence of the relative permittivity above the O–T phase boundary consistent with an increase in electrical conductivity. However, with BZ concentrations of above 2 mol%, this was no longer observed. Interestingly, the temperature-dependent dielectric data show increased conductivity at low measurements frequencies for all compositions, although the temperature at which the increase in conductivity is observed in shifted to higher temperatures with increase BZ content. Although the origin of this remains unclear, this could result from oxygen vacancies due to the enhanced K, Na, and Bi volatilization in materials with lower BZ content.[52–54] Second, there is an apparent reduction in the Curie point

with BZ, which was determined as the temperature of the maximum permittivity in temperature-dependent dielectric data. Here, T_C was shifted from 376°C for KNN–0BZ to 176°C for KNN–7BZ, showing a nearly linear decrease with a slope of approximately −28.4 ± 1.5°C/mol% BZ. In comparison, the interferroelectric phase boundary shifted to a lower temperature up to 2BZ, then slightly increased at 4BZ, and after that decreased again with increasing BZ content. Wu et al. reported a similar shift in the KNN–BLT–BZ system associated with a diffused interferroelectric phase boundary, that is, O–T and R–T for <4BZ and ≥4BZ, respectively.[19] This shift can be related to the different ionic sizes of both A and B-site cations upon increasing BZ in the system. Furthermore, the substitution of Ti^{4+} by larger Zr^{4+} cation in the B-site causes an increase in the internal chemical pressure that has the same effect as increased externally applied hydrostatic pressure, which favors the high-temperature phase with smaller unit cell.[19,55–57] In addition, an anomaly in the dielectric response of KNN–6BZ and 7BZ was observed only at 100 Hz. However, the origin of anomaly remains unclear, this could be related to the dielectric relaxation, which was previously reported in $BaTiO_3$–$BaZrO_3$ solid solution as a result of increased $BaZrO_3$ in the system.[58,59] The substitution of Zr^{4+} disrupts ferroelectricity, which is the driving force for relaxer behavior due to the cation displacements in the B site.[58]

All the investigated compositions show two phase transitions, that is, O–T or R–T, and T–C within the measured temperature range. Interestingly, in permittivity, the ΔT (= $T_{O-T/R-T} - T_C$) decreases as the T_C shifts to lower temperatures with an increasing BZ/BLT ratio. For example, ΔT between interferroelectric and paraelectric phase transition was decreased from 309°C for KNN–0BZ to 128°C for KNN–7BZ, meaning that a stability of higher temperature tetragonal phase decreased with increasing BZ/BLT ratio. In addition, as shown in Figure 1, the sudden increase in d_{33} values around T_c was diminished with decreasing ΔT.

The temperature-dependent piezoelectric response displayed a maximum at the interferroelectric phase transition, where the observed maximum d_{33} values were 176, 216, 198, 280, and 171 for KNN–0BZ, 2BZ, 4BZ, 6BZ, and 7BZ, found at 46, 23, 34, 45, and 34°C, respectively. Interestingly, despite the changes in the BZ content, the temperature of maximum d_{33} changes was found to remain in the vicinity of room temperature, displaying variations of ±10°C. Among these compositions, KNN–6BZ shows the highest maximum d_{33} of 280 pC/N and ε_r of 6402 at 45 and 215°C, respectively, which is consistent with previous reports by Wang et al.[24] That can also be related to the sudden increase in grain size, as shown in the microstructural analysis.[60] Previous researchers have attributed the observed maximum d_{33} value of KNN–6BZ composition to the convergence of R–O and O–T phase boundaries and the

formation of a new T_{PPT}.[24,61] However, it is suggested that increasing internal pressure in the B-site due to Zr cations leads to peak broadening and subsequently decreases the relative permittivity in KNN–7BZ. Importantly, although the compositional tuning can increase the d_{33} by modifying the polymorphic phase boundaries, a significant decrease in electromechanical response was observed outside of the T_{PPT}, demonstrating that temperature stability remains a substantial research topic and requires further understanding.

The maximum d_{33} values were observed at the interferroelectric phase transition for all compositions. Although previous investigations have shown that the d_{33} values increase close to the phase boundaries[62,63] due to the increased extrinsic contributions, other studies have also observed a sharp peak near the depolarization temperature.[64,65] Such peaks near T_C are related to the loss of macroscopic polarization P_3 and increase permittivity ε'_{33},[66] as expressed in the following equation:

$$d_{33} = 2Q_{11}P_3\varepsilon'_{33}\varepsilon_0 \tag{1}$$

where Q_{11} is the electrostrictive coefficient, and ε_0 is the permittivity of free space. Considering Q_{11} is approximately constant with temperature,[67,68] the increase in ε'_{33} at the phase boundary leads to an increase in d_{33}. Eventually, however, the loss in polarization reduces the piezoelectric response, resulting in the observed peak for, for example, KNN–0BZ. In contrast, KNN displays an additional peak at the lower temperature interferroelectric phase boundary, which is understood to the related to the temperature-dependent enhancement in domain wall mobility lowering the threshold stress required for domain wall motion consequently enhancing the extrinsic and intrinsic contributions[47,69] to the macroscopic piezoelectric coefficient. It is also expected that the extrinsic contributions are enhanced in the interferroelectric phase-boundary region, where multiple phases are simultaneously present.

The depolarization temperature T_d, where the macroscopic polarization is lost, cannot be readily estimated here with a fixed method for all compositions (Figure 1). For example, Schader et al. determined T_d by the inflection point in the sharp drop in d_{33}.[47] However, the depolarization temperature in low BZ content samples, that is, 0BZ and 2BZ, is closer to the Curie temperature than that of the high BZ content samples, that is, 4BZ, 6BZ, and 7BZ, due to the decrease in the sharpness of d_{33} slope with increasing BZ. For example, the estimated T_d values for 0BZ, 2BZ, 4BZ, and 6BZ were 374, 330, 262, and 199°C, respectively, whereas in the case of 7BZ, the estimation of a fixed value of T_d was not possiable due to the gradual decrease of
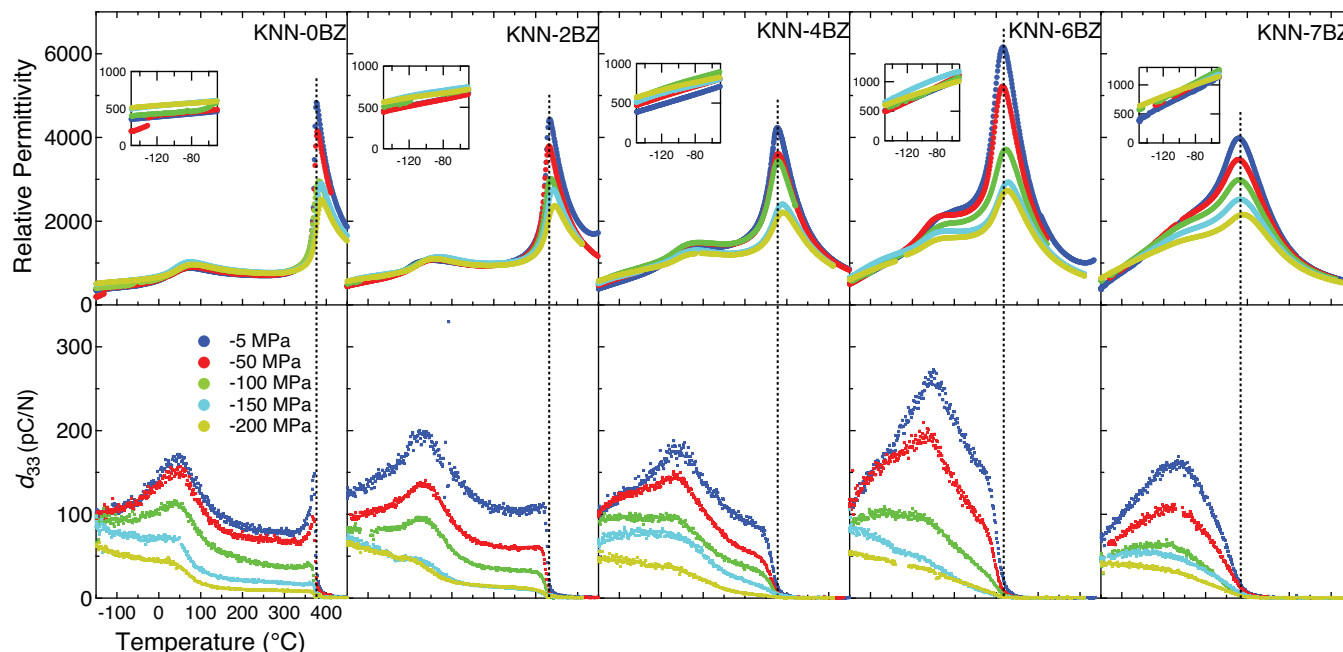
FIGURE 2 The temperature-dependent ε_r (100 kHz) (top row) and d_{33} (110 Hz) (bottom row) as a function of uniaxial compressive stress within the range from −5 to −200 MPa of KNN–100xBZ (x = 0, 2, 4, 6, and 7). The insets represent the zoomed area of the low-temperature range (i.e., from −150 to −50°C).

d_{33}. A similar observation was reported for KNN–5BZ and KNN–6BZ by Wang et al.,[24] where the decrease in c/a ratio with increasing temperature leads to a decrease in d_{33} and the broader dielectric response resulted in a more gradual d_{33} loss.

As previously mentioned, although the compositionally tuned KNN–BZ compositions display a large d_{33} value around room temperature, the piezoelectric response is found to sharply decrease with both increasing and decreasing temperature that limits the thermal stability. Interestingly, uniaxial compressive stresses have been found to improve the temperature stability range of ferroelectric phases in compositions, such as in BaTiO$_3$,[70] Pb(Zr,Ti)O$_3$,[47] and K$_{0.5}$Na$_{0.5}$NbO$_3$.[40] As such, investigating the influence of stress on the functional properties of phase-boundary-engineered KNN-compositions is critical. The temperature-dependent small-signal dielectric and piezoelectric properties were measured as a function of different constant uniaxial compressive stresses up to −200 MPa, as shown in Figure 2. Both the piezoelectric coefficients and permittivity decreased with the applied stress. Here, for low BZ contents of <4 mol%, the relative permittivity remained relatively stable with applied stress, whereas the d_{33} values show a significant decrease. This is understood to be due to the thermal activation of ferroelastic domains that results in a subsequent loss in the poled domain state and piezoelectric response. This is especially apparent near the low temperature phase boundary, where sharp loss is found. At higher BZ contents,

however, both the dielectrics and the piezoelectric properties were observed to be more stress-dependent at lower temperatures, in addition to a more gradual loss of d_{33} over a broader temperature range. This is due to the known broadening of the phase transition region, which has been suggested to be the origin of the temperature-stable ferroelectric behavior.[3] Here, the influence of the relatively large Zr^{4+} cation in the B-site to the phase stability through internal chemical pressure and smaller unit cell volume is critical, leading to a broadened dielectric response near T_c. In this investigation, however, the broader phase region did not result in enhanced thermal stability. In addition, the dotted line represents the Curie point at −5 MPa, showing the shift of T_c to higher temperatures with stress.

At lower temperatures, that is, below −50°C, the magnitudes of change in d_{33} values under stress were different from that at room temperature. For example, at −100°C, the decrease in d_{33} with stress was between 54% and 64% for all samples, whereas at room temperature, the drop in d_{33} value for maximum stress was between 70% and 80%. Thus, the extrinsic contributions are minimized at lower temperatures due to the reduced thermal energy, reducing the influence of applied stress on the overall macroscopic response.[71] Nevertheless, at lower temperatures from −150 to −50°C, the relative permittivity increased under uniaxial load for all compositions (Figure 2). Such an increase is possibly related to the increase in the number of a-axis oriented domains parallel to the applied uniaxial stress direction[72] because at lower temperatures, the applied

mechanical field is the main contributor to domain wall motion. In addition, a previous study on KNN single crystal showed an increase in the spontaneous polarization by lowering the symmetry of the crystal structure, which could be an additional possible intrinsic contribution to the relative permittivity.[29,73] However, in situ temperature–stress-dependent XRD and TEM would be required to illustrate a better understanding.

Furthermore, both interferroelectric and paraelectric phase transitions were shifted to higher temperatures under stress with varying sensitivities, depending on the composition. Such a shift in phase-transition temperatures was reported for several ferroelectric materials under uniaxial stress, for example, PZT,[47] BT,[29] and KNN,[40] where the upward shift in phase-transition temperatures was found to be associated with the mechanical stabilization of the lower symmetry, lower volume phase. The decrease in d_{33} and ε_r values under increased stress is related to the mechanical clamping of domain wall motion and ferroelastic switching,[46,74] significantly reducing both domain wall mobility and density. The degree of stress-induced variation on phase-transition temperatures and functional properties of KNN–xBZ increases with the increasing BZ content, that is, KNN–0BZ shows the lowest change in ε_r under stress, whereas KNN–7BZ shows the highest sensitivity. The difference in stress sensitivity is also observed between interferroelectric and paraelectric phase transitions, which can be related to changes in the unit cell volume. Because of the large ionic radius of Zr^{4+} (0.72 Å) compared to Ti^{4+} (0.605 Å) in the B site,[57] the internal chemical pressure favors the rhombohedral over the orthorhombic phase at room temperature, and consequently, higher sensitive phase boundaries to the uniaxial stress while heating.[55,75] At the same time, the maximum peaks of both d_{33} and ε_r were found to become broader under stress, which is related to the increase of stress-induced domain wall clamping of randomly oriented grains.[29,76,77]

The stress-dependent variation in dielectric permittivity data, as shown in Figure 2, was used to develop a stress–temperature phase diagram of the KNN–BLT–BZ system, which is essential to provide more information about the relationship between the thermal effects and electromechanical properties. In order to study the effect of stress on the phase transition, the first derivative of permittivity as a function of applied stress was determined throughout the measured temperature range, as shown in Figure 3. Temperatures below 0°C are not shown in Figure 3, as all phase transitions were found to occur at or above room temperature. The first derivative of permittivity can provide a better method for determining the phase-transition temperatures.[78,79] All samples show both an interferroelectric and a ferroelectric–paraelectric phase transition peak,
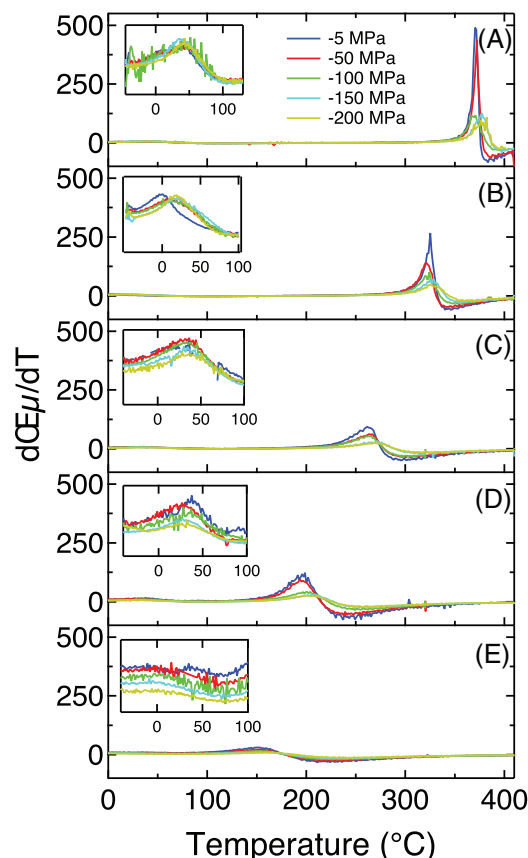
FIGURE 3 Change in permittivity as a function of temperature, $d\varepsilon_r/dT$, where (A)–(E) represent KNN–0BZ, 2BZ, 4BZ, 6BZ, and 7BZ, respectively. The inset figures show the interferroelectric phase transitions in more detail.

where the interferroelectric peaks are relatively lower than that observed at the Curie temperature. In addition, peak broadening and shifting can also be seen with increased mechanical loading. Moreover, the peak shape, position, amplitude, and width change upon increasing BZ content. For example, at the paraelectric phase transition, KNN–0BZ shows the most pronounced $d\varepsilon/dT$, which is related to high phase stability because the absence of the relatively large Zr^{4+} cation in the B site leads to less internal chemical pressure and smaller unit cell volume. Although the case of KNN–7BZ, the T–C peak shows the lowest amplitude among all compositions, where the significant change in the peak width and amplitude is related to the variation in internal chemical pressure due to the substitution of Ti^{4+} with Zr^{4+} in the B site. In addition, the difference between the paraelectric and interferroelectric phase transitions as well as the phase stability decrease with increasing Zr^{4+} content in the system. That leads to a decrease in the required temperature for phase transition.[80,81]

The stress–temperature phase diagram of the KNN–BLT–BZ system under constant uniaxial stress up to
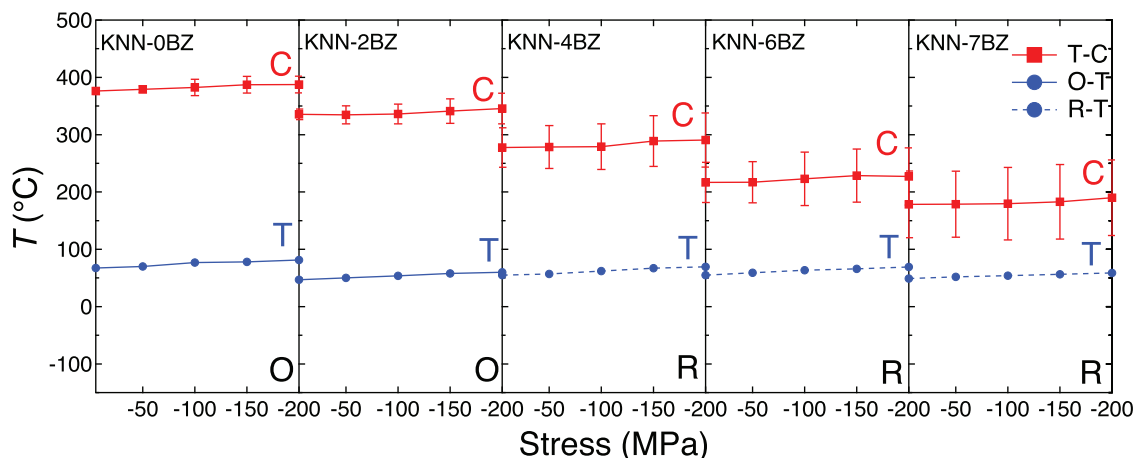
FIGURE 4 The temperature–stress phase diagram of polycrystalline KNN–xBZ (x = 0, 2, 4, 6, and 7) as a function of constant uniaxial compressive stress (from −5 to −200 MPa). The error bars stand for the integrated peak width from Figure 3.

−200 MPa is shown in Figure 4, which is based on the extracted data from Figures 2 and 3. Interestingly, the increase of BZ over BLT content causes a significant decrease in T_C, whereas the interferroelectric phase transition was relatively less affected by substitution content. This is directly related to the BZ/BLT ratio, which has a direct influence on the crystal structure[19,24] and, consequently, the phase diagram. The change in tetragonality is associated with the A-site cations, whereas such a small cation, for example, Li, leads to higher tetragonality.[82] In contrast, the stability range of the rhombohedral phase is directly related to B-site cations. For example, the substitution between Zr and Ti in the B-sites resulted in cation and lattice disorder,[55] where the structure reveals more tetragonal distortion caused by the change in the octahedral arrangement that leads toward a rhombohedral phase.[56,83] Consequently, the increase in BZ over BLT in the system decreases the ΔT between the interferroelectric and paraelectric phases and close phase transition sequence. In contrast, the error bars in Figure 4 refer to the integrated peak width from Figure 3 for the T–C phase transition.

The combined data from Figures 2 and 4 are used to illustrate the effect of the stress-dependent phase boundaries on the piezoelectric coefficient d_{33} in KNN–xBZ. Figure 5 shows a contour map of the observed d_{33} values as a function of stress, temperature, and composition. The maximum values of d_{33} were observed close to interferroelectric phase boundaries, that is, either O or R depending on composition. Similarly, an enhanced electromechanical response near structural phase boundaries has also been observed in other lead-free ferroelectrics, such as KNN,[84] NBT,[85] and BCZT,[86] where the maximum values were shown above the PPB. For example, in BCZT, this effect is related to increasing the tilted phase boundary of O–T across the convergence region.[87] However,

in the case of KNN–xBZ, the maximum value of d_{33} was located on the lower temperature, lower symmetry phase side of the interferroelectric phase boundary, and a subsequent monotonic decrease up to the Curie point. Previous investigations have suggested that this enhanced electromechanical response in the vicinity of the interferroelectric O–T and R–T phase boundaries is related to the formation of nanodomains, reduces domain wall energy, and enhances the polarization rotation.[88,89] Moreover, the d_{33} values show a continuous decrease with the applied stress with relatively higher values close to O–T and R–T phase boundaries. In the contour plot and similar to Figure 2, a significant increase of d_{33} values close to T–C in KNN–0BZ and KNN–2BZ with increasing ε_r. In contrast, the continuous decreases of d_{33} after the interferroelectric phase boundaries in KNN–4BZ, 6BZ, and 7BZ are observed due to the diffuse in the phase boundary with increasing Zr content.[19,33]

The slopes of interferroelectric and paraelectric phase boundaries in the phase diagram (Figure 4) are reported in Table 1. Generally, the slope of the interferroelectric phase transition shows higher values than the paraelectric phase transition, which is not similar to the previous study on the LKNN system, where the slopes of T_C (0.09–0.12) show higher values than $T_{O−T}$ (0.04–0.06).[40] The differences in the slope between LKNN and KNN–xBZ could be due to the differences in the chemical compositions and different doping in the KNN system. Upon adding BZ to KNN–0BZ, the O–T and T–C slopes decrease from 0.0736 and 0.0619 K/MPa to 0.0693 and 0.0543 K/MPa for KNN–2BZ, respectively. However, by adding more BZ, the slope increased to 0.0797 and 0.054 K/MPa for R–T and T–C in KNN–4BZ, respectively. However, for KNN–6BZ and 7BZ, the values of the slopes are decreased for both R–T and T–C phase boundaries. The sudden increase in the slope
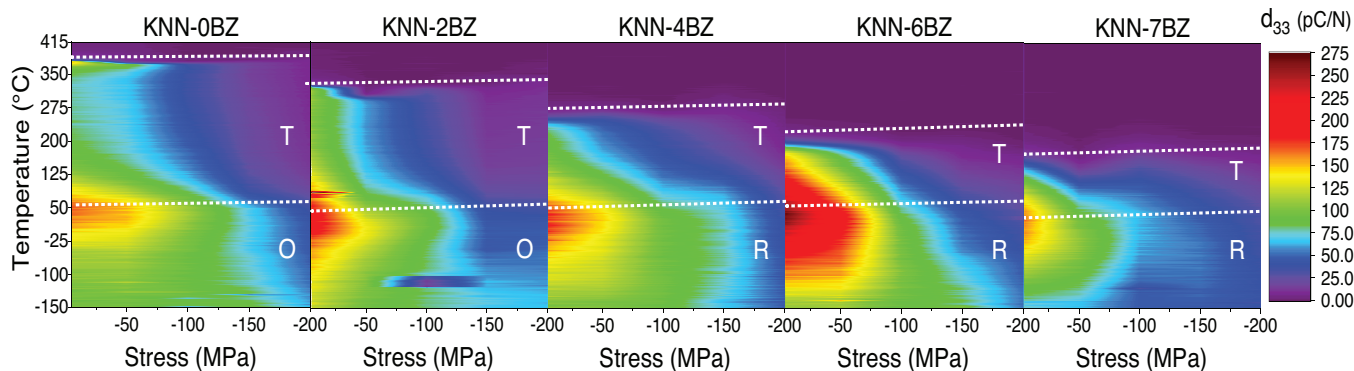
FIGURE 5 Contour plot of d_{33} of KNN–xBZ ($x = 0, 2, 4, 6,$ and 7) as a function of stress, temperature, and composition (Figure 2). White lines represent the phase transition lines from Figure 4. Some missed points are due to measurement artifacts.

TABLE 1 The shift in the interferroelectric and ferroelectric–paraelectric phase transition temperatures as a function of uniaxial compressive stress (K/MPa) for KNN–xBZ

Phase boundary	KNN–0BZ	KNN–2BZ	KNN–4BZ	KNN–6BZ	KNN–7BZ
Interferroelectric	0.0736	0.0693	0.0797	0.0717	0.0489
Ferroelectric–paraelectric	0.0619	0.0543	0.0754	0.0651	0.0566

can be related to the diffused phase transition and a new phase boundary between R and T in KNN–4BZ combined with an increase in the unit cell volume.[19] Though, there is no clear explanation why T–C phase boundary shows the same trend as the R–T phase boundary. These data provide essential information on the stability of dielectric properties and the engineered phase boundary of KNN–xBZ-based compositions under combined compressive stress and temperature field. Nevertheless, additional structural studies, such as in situ stress-dependent XRD and TEM, would be required to illustrate a better understanding of the phase transitions and crystal structure under load.

4 | CONCLUSIONS

The influence of uniaxial stress on dielectric and piezoelectric properties of 0.92KNN–(0.08 − x)BLT–xBZ (i.e., $x = 0, 0.02, 0.04, 0.06, 0.07$) was investigated within temperature range from −150 to 450°C with constant stress steps from −5 to −200 MPa, where KNN–6BZ shows the highest relative permittivity and piezoelectric coefficient of the investigated compositions. All phase boundaries were shifted to higher temperatures with increased stress. The paraelectric phase boundary shows higher stress sensitivity than interferroelectric phase boundaries. Due to domain wall clamping, the increasing compressive stress suppresses both relative permittivity and piezoelectric coefficient. The difference between T_C and T_d increases

with increasing BZ content in the system. The change of phase transition point over stress was decreased with BZ content. However, due to the diffused phase transition and a new MPB between R and T in KNN–4BZ, the rate of change increased between KNN–2BZ and KNN–4BZ. This work shows the effect of the mechanical and thermal field on the phase stability and the electromechanical properties of BLT–BZ-doped KNN-based compositions.

CONFLICT OF INTEREST
The authors declare no conflict of interest.

ORCID
Ahmed Gadelmawla https://orcid.org/0000-0002-5939-9277
Ke Wang https://orcid.org/0000-0001-9840-2427
Jing-Feng Li https://orcid.org/0000-0001-7719-9060
Neamul H. Khansur https://orcid.org/0000-0001-8769-3329

REFERENCES

1. Rödel J, Webber KG, Dittmer R, Jo W, Kimura M, Damjanovic D. Transferring lead-free piezoelectric ceramics into application. J Eur Ceram Soc. 2015;35(6):1659–81.

2. Coondoo I, Panwar N, Kholkin A. Lead-free piezoelectrics: current status and perspectives. J Adv Dielectr. 2013;03(02):1330002.

3. Wang K, Yao F-Z, Jo W, Gobeljic D, Shvartsman VV, Lupascu DC, et al. Temperature-insensitive $(K,Na)NbO_3$-based lead-free piezoactuator ceramics. Adv Funct Mater. 2013;23(33):4079–86.

4. Li J-F, Wang K, Zhu F-Y, Cheng L-Q, Yao F-Z. $(K,Na)NbO_3$-based lead-free piezoceramics: fundamental aspects, processing technologies, and remaining challenges. J Am Ceram Soc. 2013;96(12):3677–96.

5. Saito Y, Takao H, Tani T, Nonoyama T, Takatori K, Homma T, et al. Lead-free piezoceramics. Nature. 2004;432(7013):84–7.

6. Berlincourt DA, Curran DR, Jaffe H. Piezoelectric and piezomagnetic materials and their function in transducers. In: Physical acoustics. Amsterdam: Elsevier; 1964. p. 169–270.

7. Wang K, Li J-F. Domain engineering of lead-free Li-modified $(K,Na)NbO_3$ polycrystals with highly enhanced piezoelectricity. Adv Funct Mater. 2010;20(12):1924–9.

8. Wang K, Li J-F. Low-temperature sintering of Li-modified $(K,Na)NbO_3$ lead-free ceramics: sintering behavior, microstructure, and electrical properties. J Am Ceram Soc. 2010;93(4):1101–7.

9. Wang K, Li J-F. $(K, Na)NbO_3$-based lead-free piezoceramics: phase transition, sintering and property enhancement. J Adv Ceram. 2012;1(1):24–37.

10. Wang K, Li J-F, Liu N. Piezoelectric properties of low-temperature sintered Li-modified $(Na, K)NbO_3$ lead-free ceramics. Appl Phys Lett. 2008;93(9):92904.

11. Zhang M-H, Wang K, Zhou J-S, Zhou J-J, Chu X, Lv X, et al. Thermally stable piezoelectric properties of $(K, Na)NbO_3$-based lead-free perovskite with rhombohedral-tetragonal coexisting phase. Acta Mater. 2017;122:344–51.

12. Zhang M-H, Wang K, Du Y-J, Dai G, Sun W, Li G, et al. High and temperature-insensitive piezoelectric strain in alkali niobate lead-free perovskite. J Am Chem Soc. 2017;139(10):3889–95.

13. Zhang M-H, Thong HC, Lu YX, Sun W, Li J-F, Wang K. $(K,Na)NbO_3$-based lead-free piezoelectric materials: an encounter with scanning probe microscopy. J Korean Ceram Soc. 2017;54(4):261–71.

14. Ge W, Ren Y, Zhang J, Devreugd CP, Li J, Viehland D. A monoclinic-tetragonal ferroelectric phase transition in lead-free $(K_{0.5}Na_{0.5})NbO_3$-x%LiNbO_3 solid solution. J Appl Phys. 2012;111(10):103503.

15. Wang K, Li J-F. Analysis of crystallographic evolution in $(Na,K)NbO_3$-based lead-free piezoceramics by x-ray diffraction. Appl Phys Lett. 2007;91(26):262902.

16. Iamsasri T, Tutuncu G. Chunmanus Uthaisar, Soodkhet Pojprapai & Jacob L. Jones. J Mater Sci. 2013;48:6905–10. https://doi.org/10.1007/s10853-013-7495-2

17. Lv X, Zhu J, Xiao D, Zhang X-X, Wu J. Emerging new phase boundary in potassium sodium-niobate based ceramics. Chem Soc Rev. 2020;49(3):671–707.

18. Zhang Y, Li J-F. Review of chemical modification on potassium sodium niobate lead-free piezoelectrics. J Mater Chem C. 2019;7(15):4284–303.

19. Wu M, Fang L, Liu L, Zhou X, Huang Y, Li Y. Diffusion phase transition and ferroelectric properties of $0.92K_{0.5}Na_{0.5}NbO_3$–$(0.08–x)Bi_{0.5}Li_{0.5}Ti_{O3}$–xBaZrO_3 ceramics. Mater Chem Phys. 2012;132(2–3):1015–8.

20. Guo Y, Kakimoto K, Ohsato H. Phase transitional behavior and piezoelectric properties of $(Na_{0.5}K_{0.5})NbO_3$–LiNbO_3 ceramics. Appl Phys Lett. 2004;85(18):4121–3.

21. Wang R, Bando H, Katsumata T, Inaguma Y, Taniguchi H, Itoh M. Tuning the orthorhombic-rhombohedral phase transition temperature in sodium potassium niobate by incorporating barium zirconate. Phys Status Solidi RRL. 2009;3(5):142–4.

22. Wang X, Wu J, Xiao D, Zhu J, Cheng X, Zheng T, et al. Giant piezoelectricity in potassium-sodium niobate lead-free ceramics. J Am Chem Soc. 2014;136(7):2905–10.

23. Jaffe B, Cook WR, Jaffe H. Piezoelectric ceramics. London: Academic Press; 1971. JCPDS 71-2171.

24. Wang R, Wang K, Yao F, Li J-F, Schader FH, Webber KG, et al. Temperature stability of lead-free niobate piezoceramics with engineered morphotropic phase boundary. J Am Ceram Soc. 2015;98(7):2177–82.

25. Shkuratov SI, Baird J, Antipov VG, Lynch CS, Zhang S, Chase JB, et al. Giant power density produced by PIN–PMN–PT ferroelectric single crystals due to a pressure induced polar-to-nonpolar phase transformation. J Mater Chem A. 2021;9(20):12307–19.

26. Rossetti GA, Cross LE, Kushida K. Stress induced shift of the Curie point in epitaxial $PbTiO_3$ thin films. Appl Phys Lett. 1991;59(20):2524–6.

27. Zeches RJ, Rossell MD, Zhang JX, Hatt AJ, He Q, Yang C-H, et al. A strain-driven morphotropic phase boundary in $BiFeO_3$. Science. 2009;326(5955):977–80.

28. Arlt G, Hennings D, With G de. Dielectric properties of fine-grained barium titanate ceramics. J Appl Phys. 1985;58(4):1619–25.

29. Schader FH, Aulbach E, Webber KG, Rossetti GA. Influence of uniaxial stress on the ferroelectric-to-paraelectric phase change in barium titanate. J Appl Phys. 2013;113(17):174103.

30. Forsbergh PW. Effect of a two-dimensional pressure on the Curie point of barium titanate. Phys Rev. 1954;93(4):686–92.

31. Merz WJ. The effect of hydrostatic pressure on the Curie point of barium titanate single crystals. Phys Rev. 1950;78(1):52–4.

32. Hayward SA, Salje EKH. The pressure temperature phase diagram of $BaTiO_3$ a macroscopic description of the low-temperature behaviour. J Phys: Condens Matter. 2002;14(36):L599–604.

33. Veerapandiyan V, Popov MN, Mayer F, Spitaler J, Svirskas S, Kalendra V, et al. Origin of relaxor behavior in barium-titanate-based lead-free perovskites. Adv Electron Mater. 2022;8(2):2100812.

34. Zuo R, Fu J. Rhombohedral-tetragonal phase coexistence and piezoelectric properties of $(NaK)(NbSb)O_3$-LiTaO_3-BaZrO_3 lead-free ceramics. J Am Ceram Soc. 2011;94(5):1467–70.

35. Khansur NH, Martin A, Riess K, Nishiyama H, Hatano K, Wang K, et al. Stress-modulated optimization of polymorphic phase transition in Li-doped $(K,Na)NbO_3$. Appl Phys Lett. 2020;117(3):32901.

36. Khansur NH, Eckstein UR, Bergler M, Martin A, Wang K, Li J-F, et al. In situ combined stress- and temperature-dependent Raman spectroscopy of Li-doped $(Na,K)NbO_3$. J Am Ceram Soc. 2022;105(4):2735–43.

37. Kakimoto K, Sumi T, Kagomiya I. Pressure-dependent raman scattering spectrum of piezoelectric (Li,Na,K)NbO$_3$ lead-free ceramics. Jpn J Appl Phys. 2010;49(9):09MD10.

38. Schader FH, Wang Z, Hinterstein M, Daniels JE, Webber KG. Stress-modulated relaxor-to-ferroelectric transition in lead-free (Na$_{1/2}$Bi$_{1/2}$)TiO$_3$−BaTiO$_3$ ferroelectrics. Phys Rev B. 2016;93(13):134111.

39. Schader FH, Morozov M, Wefring ET, Grande T, Webber KG. Mechanical stability of piezoelectric properties in ferroelectric perovskites. J Appl Phys. 2015;117(19):194101.

40. Martin A, Khansur NH, Eckstein U, Riess K, Kakimoto K, Webber KG. High temperature piezoelectric response of polycrystalline Li-doped (K,Na)NbO$_3$ ceramics under compressive stress. J Appl Phys. 2020;127(11):114101.

41. Zhang H, Groh C, Zhang Q, Jo W, Webber KG, Rödel J. Large strain in relaxor/ferroelectric composite lead-free piezoceramics. Adv Electron Mater. 2015;1(6):1500018.

42. Webber KG, Vögler M, Khansur NH, Kaeswurm B, Daniels JE, Schader FH. Review of the mechanical and fracture behavior of perovskite lead-free ferroelectrics for actuator applications. Smart Mater Struct. 2017;26(6):63001.

43. Martin A, Kakimoto K, Hatano K, Doshida Y, Webber KG. Ferroelastic behavior across the orthorhombic-to-tetragonal phase transition region of NKN-based lead-free ferroelectrics. J Appl Phys. 2017;122(20):204102.

44. Martin A, Uršič H, Rojac T, Webber KG. Direct observation of the stress-induced domain structure in lead-free (Na$_{1/2}$Bi$_{1/2}$)TiO$_3$-based ceramics. Appl Phys Lett. 2019;114(5):52901.

45. Schindelin J, Arganda-Carreras I, Frise E, Kaynig V, Longair M, Pietzsch T, et al. Fiji: an open-source platform for biological-image analysis. Nat Methods. 2012;9(7):676–82.

46. Ehmke MC. Ferroelastic domains in lead-free barium zirconate titanate – barium calcium titanate piezoceramics. [Dissertation]. West Lafayette, Indiana: Purdue University; 2014.

47. Schader FH, Isaia D, Weber M, Aulbach E, Webber KG. High-temperature stress-dependent piezoelectric and dielectric coefficient of soft Pb(Zr,Ti)O3. J Mater Sci. 2018;53(5):3296–308.

48. Wang Y, Damjanovic D, Klein N, Hollenstein E, Setter N. Compositional inhomogeneity in Li- and Ta-modified (K, Na)NbO$_3$ ceramics. J Am Ceram Soc. 2007;90(11):3485–9.

49. Wang Y, Damjanovic D, Klein N, Setter N. High-temperature instability of Li- and Ta-modified (K,Na)NbO$_3$ piezoceramics. J Am Ceram Soc. 2008;91(6):1962–70.

50. Martin A, Kakimoto K. Effect of domain structure on the mechanical and piezoelectric properties of lead-free alkali niobate ceramics. Jpn J Appl Phys. 2014;53(9S):09PB09.

51. Matsubara M, Yamaguchi T, Kikuta K, Hirano S. Effect of Li substitution on the piezoelectric properties of potassium sodium niobate ceramics. Jpn J Appl Phys. 2005;44(8):6136–42.

52. Liu L, Huang Y, Su C, Fang L, Wu M, Hu C, et al. Space-charge relaxation and electrical conduction in K$_{0.5}$Na$_{0.5}$NbO$_3$ at high temperatures. Appl Phys A. 2011;104(4):1047–51.

53. Liu L, Fan H, Fang L, Chen X, Dammak H, Thi MP. Effects of Na/K evaporation on electrical properties and intrinsic defects in Na$_{0.5}$K$_{0.5}$NbO$_3$ ceramics. Mater Chem Phys. 2009;117(1):138–41.

54. Gadelmawla A, Riess K, Birkenstock J, Hinterstein M, Webber KG, Khansur NH. Effect of varying Bi content on the temperature-dependent mechanical, dielectric, and structural properties of nominal Na$_{1/2}$Bi$_{1/2}$TiO$_3$. J Appl Phys. 2021;130(18):185106.

55. Zhong W, Vanderbilt K, Rabe KM. First-principles theory of ferroelectric phase transitions for perovskites: the case of BaTiO$_3$. Phys Rev B: Condens Matter. 1995;52(9):6301–12.

56. Liu L, Huang Y, Li Y, Fang L, Dammak H, Fan H, et al. Orthorhombic to tetragonal structural phase transition in Na$_{0.5}$K$_{0.5}$NbO$_3$-based ceramics. Mater Lett. 2012;68:300–2.

57. Shannon RD. Revised effective ionic radii and systematic studies of interatomic distances in halides and chalcogenides. Acta Cryst A. 1976;32(5):751–67.

58. Veerapandiyan V, Popov MN, Mayer F, Spitaler J, Svirskas S, Kalendra V, et al. Origin of relaxor behavior in barium-titanate-based lead-free perovskites. Adv Electron Mater. 2022;8(2):2100812.

59. Maiti T, Guo R, Bhalla AS. The evolution of relaxor behavior in Ti[sup 4+] doped BaZrO[sub 3] ceramics. J Appl Phys. 2006;100(11):114109.

60. Randall CA, Kim N, Kucera J-P, Cao W, Shrout TR. Intrinsic and extrinsic size effects in fine-grained morphotropic-phase-boundary lead zirconate titanate ceramics. J Am Ceram Soc. 1998;81(3):677–88.

61. Duong TA, Erkinov F, Nguyen HTK, Ahn CW, Kim BW, Han H-S, et al. Temperature insensitive piezoelectric properties on the morphotropic phase boundary of BaZrO$_3$-modified lead-free KNN-BLT ceramics. J Electroceram. 2020;45(4):164–71.

62. Acosta M, Novak N, Jo W, Rödel J. Relationship between electromechanical properties and phase diagram in the Ba(Zr$_{0.2}$Ti$_{0.8}$)O$_3$–x(Ba$_{0.7}$Ca$_{0.3}$)TiO$_3$ lead-free piezoceramic. Acta Mater. 2014;80:48–55.

63. Liu H, Chen J, Huang H, Fan L, Ren Y, Pan Z, et al. Role of reversible phase transformation for strong piezoelectric performance at the morphotropic phase boundary. Phys Rev Lett. 2018;120(5):55501.

64. Kaeswurm B, Schader FH, Webber KG. Ferroelectric, ferroelastic, piezoelectric, and dielectric properties of lead zirconate titanate from −150°C to 350°C. Ceram Int. 2018;44(2):2358–63.

65. Li F, Xu Z, Wei X, Yao X. Determination of temperature dependence of piezoelectric coefficients matrix of lead zirconate titanate ceramics by quasi-static and resonance method. J Phys D: Appl Phys. 2009;42(9):95417.

66. Sundar V, Newnham RE. Electrostriction and polarization. Ferroelectrics. 1992;135(1):431–46.

67. Weaver PM, Cain MG, Stewart M. Temperature dependence of high field electromechanical coupling in ferroelectric ceramics. J Phys D: Appl Phys. 2010;43(16):165404.

68. Dittmer R, Webber KG, Aulbach E, Jo W, Tan X, Rödel J. Optimal working regime of lead–zirconate–titanate for actuation applications. Sens Actuators A. 2013;189:187–94.

69. Liu G, Zhang S, Jiang W, Cao W. Losses in ferroelectric materials. Mater Sci Eng R: Rep. 2015;89:1–48.

70. JAFFE H, Berlincourt D, McKee JM. Effect of pressure on the Curie temperature of polycrystalline ceramic barium titanate. Phys Rev. 1957;105(1):57–8.

71. Zhang XL, Chen ZX, Cross LE, Schulze WA. Dielectric and piezoelectric properties of modified lead titanate zirconate ceramics from 4.2 to 300 K. J Mater Sci. 1983;18(4): 968–72.

72. Merz WJ. The electric and optical behavior of $BaTiO_3$ single-domain crystals. Phys Rev. 1949;76(8):1221–5.

73. Ishizawa N, Wang J, Sakakura T, Inagaki Y, Kakimoto K. Structural evolution of $Na_{0.5}K_{0.5}NbO_3$ at high temperatures. J Solid State Chem. 2010;183(11):2731–8.

74. Ehmke MC, Schader FH, Webber KG, Rödel J, Blendell JE, Bowman KJ. Stress, temperature and electric field effects in the lead-free (Ba,Ca)(Ti,Zr)O_3 piezoelectric system. Acta Mater. 2014;78:37–45.

75. Di Zhan, Xu Q, Huang D-P, Liu H-X, Chen W, Zhang F. Contributions of intrinsic and extrinsic polarization species to energy storage properties of $Ba_{0.95}Ca_{0.05}Zr_{0.2}Ti_{0.8}O_3$ ceramics. J Phys Chem Solids. 2018;114:220–7.

76. Pramanick A, Damjanovic D, Daniels JE, Nino JC, Jones JL. Origins of electro-mechanical coupling in polycrystalline ferroelectrics during subcoercive electrical loading. J Am Ceram Soc. 2011;94(2):293–309.

77. Damjanovic D, Demartin M. The Rayleigh law in piezoelectric ceramics. J Phys D: Appl Phys. 1996;29(7):2057–60.

78. Serghei A, Zhao W, Miranda D, Russell TP. Curie transitions for attograms of ferroelectric polymers. Nano Lett. 2013;13(2):577–80.

79. Gadelmawla A, Dobesh D, Eckstein U, Grübl O, Ehmke M, Cicconi MR, et al. Influence of stress on the electromechanical properties and the phase transitions of lead-free $(1-x)Ba(Zr_{0.2}Ti_{0.8})O_3–x(Ba_{0.7}Ca_{0.3})TiO_3$. J Mater Sci. 2022;57(35):16581–99.

80. Sawada S, Shirane G. Specific heat and thermal expansion of $BaTiO_3$. J Phys Soc Jpn. 1949;4(1):52–6.

81. Shirane G, Takeda A. Transition energy and volume change at three transitions in barium titanate. J Phys Soc Jpn. 1952;7(1):1–4.

82. Bilc DI, Singh DJ. Frustration of tilts and A-site driven ferroelectricity in $KNbO_3$-$LiNbO_3$ alloys. Phys Rev Lett. 2006;96(14):147602.

83. Ghita M, Fornari M, Singh DJ, Halilov SV. Interplay between A-site and B-site driven instabilities in perovskites. Phys Rev B. 2005;72(5):54114.

84. Lv X, Wu J, Xiao D, Zhu J, Zhang X. Structural evolution of the R-T phase boundary in KNN-based ceramics. J Am Ceram Soc. 2018;101(3):1191–200.

85. Zhang Q, Zhao X, Sun R, Luo H. Crystal growth and electric properties of lead-free NBT-BT at compositions near the morphotropic phase boundary. Phys Status Solidi A. 2011;208(5):1012–20.

86. Acosta M, Khakpash N, Someya T, Novak N, Jo W, Nagata H, et al. Origin of the large piezoelectric activity in $(1-x)Ba(Zr_{0.2}Ti_{0.8})O_3-x(Ba_{0.7}Ca_{0.3})TiO_3$ ceramics. Phys Rev B. 2015;91(10):104108.

87. Gao J, Hu X, Le Zhang, Li F, Zhang L, Wang Y, et al. Major contributor to the large piezoelectric response in $(1-x)Ba(Zr_{0.2}Ti_{0.8})O_3 - x(Ba_{0.7}Ca_{0.3})TiO_3$ ceramics: domain wall motion. Appl Phys Lett. 2014;104(25):252909.

88. Wang X, Wu J, Dkhil B, Xu B, Wang X, Dong G, et al. Enhanced electrocaloric effect near polymorphic phase boundary in lead-free potassium sodium niobate ceramics. Appl Phys Lett. 2017;110(6):63904.

89. Wang R, Xie R-J, Hanada K, Matsusaki K, Kawanaka H, Bando H, et al. Enhanced piezoelectricity around the tetragonal/orthorhombic morphotropic phase boundary in (Na,K)NbO_3–$ATiO_3$ solid solutions. J Electroceram. 2008;21(1–4):263–6.

SUPPORTING INFORMATION

Additional supporting information can be found online in the Supporting Information section at the end of this article.